Supporting Information (SI) for

TEM Analysis of Dicarboxylic Acid–Induced Transition from Unilamellar to Multilamellar MEL-A Vesicles

Tran Ngoc Linh,*[a] Hirohmi Watanabe,[a] Takashi Arimura[b] and Masato Kawasaki[c]

[a] Research Institute for Sustainable Chemistry, National Institute of Advanced Industrial Science and Technology (AIST), 3-11-32, Kagamiyama, Higashihiroshima, Hiroshima 739-0046, Japan.
[b] Open Innovation Laboratory for Food and Medicinal Resource Engineering (FoodMed-OIL), National Institute of Advanced Industrial Science and Technology (AIST), Laboratory of Advanced Research D, University of Tsukuba, Tsukuba, Ibaraki 305-0006, Japan.
[c] Institute of Materials Structure Science, Inter-University Research Institute Corporation High Energy Accelerator Research Organization (KEK), 1-1 Oho, Tsukuba, Ibaraki 305-0801, Japan.

* Corresponding author:
Tran Ngoc Linh
Organic Materials Diagnosis Group, Research Institute for Sustainable Chemistry, National Institute of Advanced Industrial Science and Technology, 3-11-32 Kagamiyama, Higashihiroshima, Hiroshima 739-0046, Japan.
Tel: (+81) 50-3522-3146
E-mail: tran.linh@aist.go.jp.

Experiments and Methods

1. Preparation of MEL-A

The **MEL-A** was synthesized according to the reported procedure[S1], except that the glucose concentration (w/v) was increased from 4% to 10%, and the incubation time was fixed at 8 days. The strain *Pseudozyma antarcticus* was used as the source organism and cultured under conditions in which glucose served as the sole carbon source. Briefly, the strain was cultivated in YM medium (3 g L^{-1} yeast extract, 3 g L^{-1} malt extract, 5 g L^{-1} peptone, and 10 g L^{-1} glucose) as a seed culture at 25 °C for 2 days with reciprocal shaking at 200 rpm. GC-MS analysis revealed that the acyl substituents of **MEL-A** consisted of C8:0 (3.0%), C10:0 (43.3%), C10:1 (7.1%), C12:0 (41.4%), C14:0 (3.9%), and C16:0 (1.3%). These compositional data demonstrate the intrinsic molecular heterogeneity arising from variations in both fatty-acid chain length and degree of unsaturation.

2. Pyrene Fluorescence Probe Methods

2.1. Determination of the Critical Aggregation Concentration (CAC)

The CAC value of **MEL-A** in aqueous solution was determined by a fluorescence probe method using pyrene as a hydrophobic probe, according to a previously reported method.[S2] Fluorescence measurements were carried out on a Hitachi F-2700 spectrofluorometer (Hitachi Ltd., Japan) at 25ºC with an excitation wavelength (λ_{ex}) of 335 nm. A solution of **MEL-A** in ethanol was added to an aqueous solution containing pyrene (concentration of 2.0×10^{-6} M). The CAC was determined by plotting the intensity ratio of the third vibronic band (I_3, 384 nm) to the first vibronic band (I_1, 373 nm) in the pyrene fluorescence emission spectrum as a function of the **MEL-A** concentration. All measurements were performed in triplicate (n = 3), representative data are shown in Fig. S1.

2.2. Evaluation of the Hydrophobic Environment Formed by MEL-A Vesicles

The relative intensity of the pyrene monomer fluorescence (the I_3/I_1 ratio) is widely used index for characterizing the microenvironmental effects on pyrene fluorescence.[S2] The I_3/I_1 ratio generally increases as the dipole moment of the solvent decreases. In aqueous buffer solutions at pH 7 or pH 4 containing **MEL-A** (10^{-3} M or 10^{-4} M), the I_3/I_1 ratios of the pyrene monomer fluorescence were in the range of 1.05–1.06. These values were higher than the ratio observed in chloroform (I_3/I_1 ratio = 0.79), indicating that the hydrophobic domains formed by **MEL-A** vesicles in aqueous buffer provide a more hydrophobic environment than chloroform (Table S2).

Rationale for Fluorescent Probe Selection. In this study, we aimed to evaluate the local environment surrounding the hydroxyl groups of the erythritol moiety in **MEL-A** vesicles, with particular focus on the two hydroxyl groups located closer to the hydrophobic region. A key issue

in this context is whether water molecules can access the vicinity of these hydroxyl groups, i.e., whether effective hydrogen bonding is possible, which is closely related to hydrophobic exclusion.

For this purpose, pyrene was employed as a fluorescent probe. Pyrene is known to preferentially partition into hydrophobic domains lacking water within self-assembled structures and does not directly report polarity or hydration at polar–non-polar interfaces. Accordingly, in the present study, pyrene fluorescence was not interpreted as a direct measure of interfacial hydration, but rather as a complementary probe to assess the presence of low-polarity microenvironments within **MEL-A** assemblies. All data were interpreted with careful consideration of the characteristics and inherent limitations of the pyrene fluorescence method.

In contrast, Laurdan is a fluorescent probe sensitive to dipolar relaxation of water molecules in the excited state and is therefore well suited for probing hydration and phase behaviour in interfacial regions where water is already present, typically near the glycerol–carbonyl region of lipid membranes. Laurdan fluorescence is governed by dipolar relaxation processes occurring during the excited-state lifetime, which require the presence of reorientable water molecules.[S3,S4] Consequently, Laurdan predominantly reflects hydration dynamics in water-accessible regions and does not directly report hydrophobic exclusion in poorly hydrated environments.

Based on these considerations, we concluded that the use of pyrene provides information more directly relevant to the objectives of this study, namely, the hydrophobicity and restricted hydrogen-bonding capability in the vicinity of the erythritol hydroxyl groups within **MEL-A** vesicles.

3. Preparation of MEL-A Vesicles in Buffered Solutions

An aqueous buffer solution at pH 7 was prepared from 0.05 M HEPES and 0.01 M KOH. An aqueous buffer solution at pH 4 was prepared from 0.05 M glycine and 0.005 M acetic acid. A **MEL-A** solution in ethanol was gently added dropwise to the buffer solution under mild stirring, resulting in the formation of a **MEL-A** vesicle suspension. To investigate the influence of carboxylic acids on **MEL-A** vesicles, an aqueous solution containing various dicarboxylic acids (including oxalic acid, maleic acid, fumaric acid, malonic acid, among others) was introduced into the vesicle suspension. The resulting mixture was incubated at 25ºC for 24 h prior to measurements.

4. Measurement of Hydrodynamic Diameter and Zeta Potential

The hydrodynamic diameter was measured by dynamic light scattering (DLS) using an ELSZneo instrument (Otsuka Electronics, Japan) at 25°C. The hydrodynamic diameter (*D*) and polydispersity index (PDI) are reported as the mean ± standard deviation (SD) of at least three independent experiments.

The zeta potential (ζ-potential) was measured using the same instrument (ELSZneo) at 25°C by laser Doppler electrophoresis. ζ-potential values were calculated using the Smoluchowski equation and the values are reported as the mean ± SD of at least three independent experiments.

5. Liquid Cell Transmission Electron Microscopy (LC-TEM) Measurements

A small aliquot of the vesicle suspension was introduced into a liquid cell (K-kit, Bio MA-TEK) via capillary action, followed by sealing with a water-resistant adhesive. TEM observations were performed using a JEM-ARM200F NEOARMex instrument (JEOL, Japan) at an accelerating voltage of 200 kV. The obtained TEM images were analyzed using ImageJ software (National Institute of Health, USA).

6. Cryogenic Transmission Electron Microscopy (Cryo-TEM) Measurements

An aliquot (3 µL) of the vesicle suspension was applied onto a carbon-supported copper grid and subsequently loaded into an FEI Vitrobot plunge-freezing system. The grid was equilibrated and blotted for approximately 15 s under controlled environmental conditions (18°C, 100% relative humidity), after which it was rapidly vitrified by plunged into liquid ethane precooled with liquid nitrogen to ~90 K. The vitrified specimen was transferred under cryogenic conditions to a cryo-holder mounted on a cryo-transfer stage submerged in liquid nitrogen. Cryo-TEM imaging was performed at the Cryo-EM Facility of the High Energy Accelerator Research Organization (KEK, Tsukuba, Ibaraki, Japan) using a Talos Arctica transmission electron microscope (Thermo Fisher Scientific, USA) operated at an accelerating voltage of 200 kV. Micrographs were processed and analyzed using the ImageJ software package.

7. NMR Experiments

NMR spectra were acquired on a JEOL 400YH Fourier-transform spectrometer operating at 400 MHz at 25ºC. Chemical shifts (δ) for the ^{1}H NMR spectra are reported in parts per million (ppm) and were referenced to using 1,1,2,2,3,3-hexadeutero-3-(trimethylsilyl)propane-1-sulfonate-d_6 sodium salt (DSS-d_6, δ = 0 ppm) as an internal standard. Coupling constants (J) are reported in hertz (Hz). The ^{1}H NMR spectra of **MEL-A** and *meso*-erythritol are shown in Fig. S2 and Fig. S3, respectively.

8. Vesicle Diameter Distributions and Lamellar Layer Number Histograms

At pH 4, cryo-TEM images of at least 56 vesicles (ranging from 56 to 233 vesicles) were analysed for each dicarboxylic acid. The number of lamellar layers for each vesicle observed in the cryo-TEM micrographs was counted visually. Based on these measurements, histograms of

the lamellar layer number were constructed. The numbers of vesicles analysed were as follows: oxalic acid (233), maleic acid (204), fumaric acid (96), malonic acid (108), succinic acid (56), glutaric acid (77), adipic acid (154), and propionic acid (202).

The vesicle diameter distributions measured by DLS are shown in Fig. S6, and the lamellar layer number histograms are presented in Fig. S7.

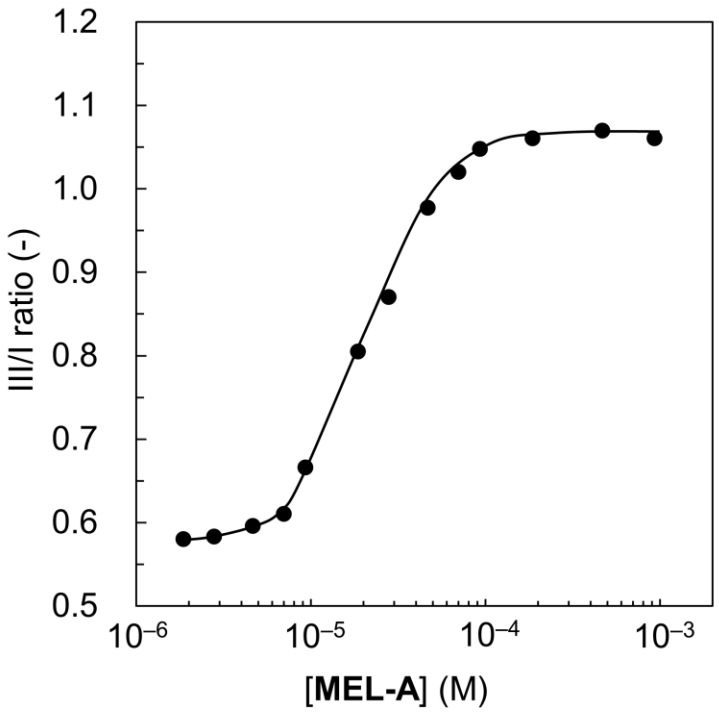

Fig. S1. Plot of the I_3/I_1 ratio of pyrene monomer fluorescence as a function of **MEL-A** concentration in water at 25°C; [pyrene] = 2.0×10^{-6} M, λ_{ex} = 335 nm.

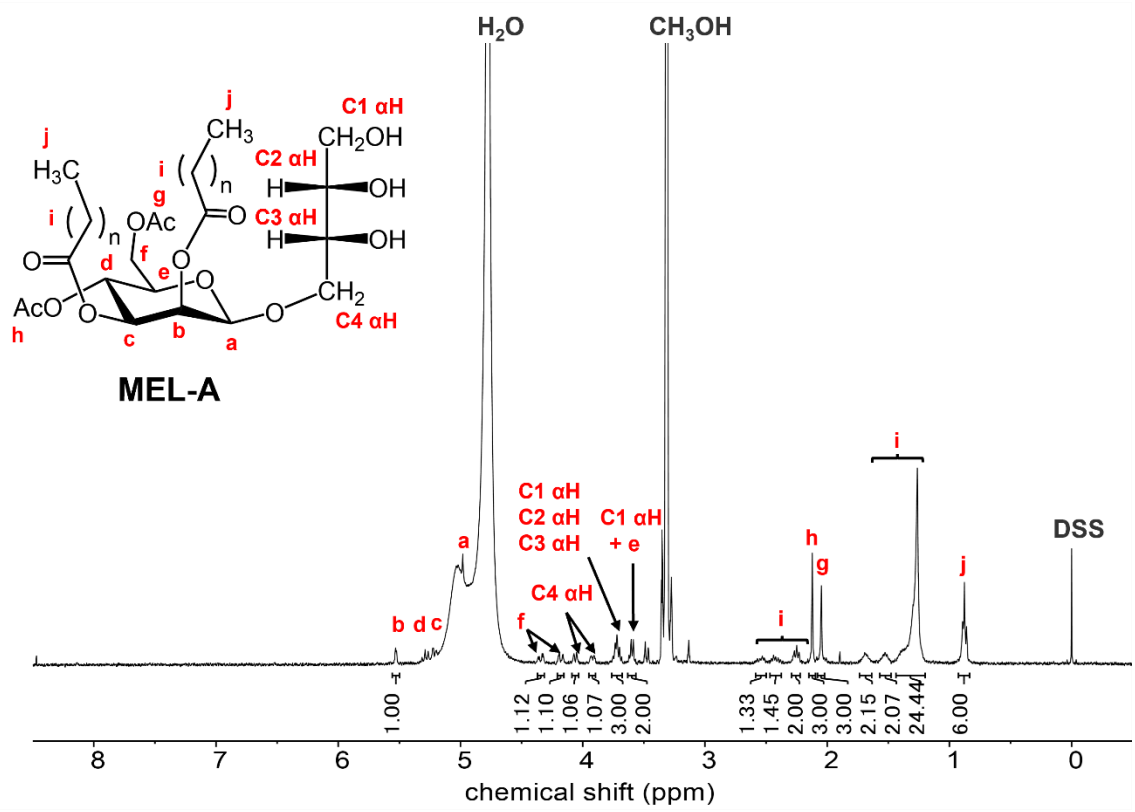

Fig. S2. ^{1}H NMR spectrum of **MEL-A** (400 MHz, 25°C, D_2O/CD_3OD = 40:60).

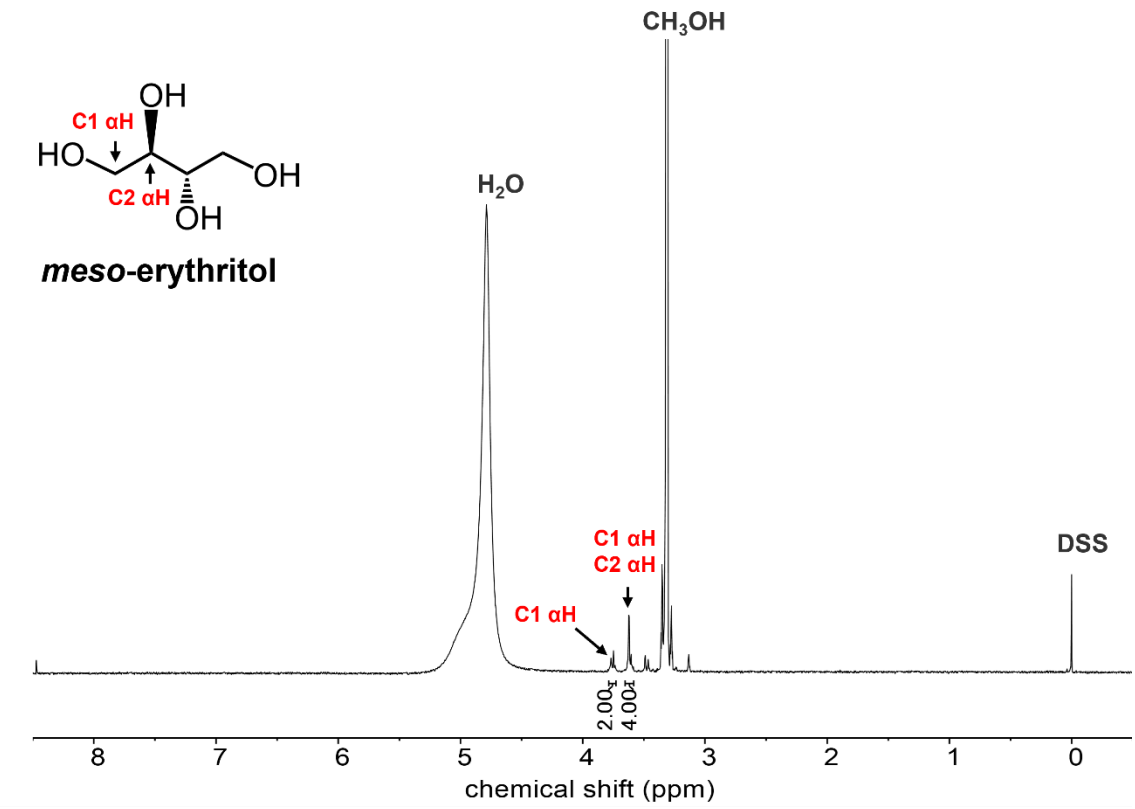

Fig. S3. ^{1}H NMR spectrum of *meso*-erythritol (400 MHz, 25°C, D_2O/CD_3OD = 40:60).

Table S1. Calculated species distributions of the undissociated form H_2A (α_0), the monovalent anionic form HA^- (α_1), and the divalent anionic form A^{2-}(α_2) at pH 7 and pH 4, based on the pK_{a1} and pK_{a2} values of dicarboxylic acids

Dicarboxylic acids	pK_{a1}	pK_{a2}	pH 7			pH 4		
			α_0	α_1	α_2	α_0	α_1	α_2
Oxalic acid	1.27	4.27	0	0.2	99.8	0.1	64.9	35.0
Maleic acid	1.91	6.33	0	17.6	82.4	0.8	98.7	0.5
Fumaric acid	3.09	4.60	0	0.4	99.6	9.0	72.8	18.2
Malonic acid	2.83	5.70	0	4.8	95.2	6.2	92.0	1.8
Succinic acid	4.21	5.64	0	4.2	95.8	61.3	37.8	0.9
Glutaric acid	4.34	5.42	0	2.6	97.4	67.8	31.0	1.2
Adipic acid	4.42	5.41	0	2.5	97.5	71.7	27.3	1.0

The ionization of dicarboxylic acid in aqueous solution can be described by the following equations:

$H_2A \rightleftharpoons H^+ + HA^-$ $\quad K_{a1}$

$HA^- \rightleftharpoons H^+ + A^{2-}$ $\quad K_{a2}$

In this context, H_2A, HA^-, A^{2-} denote the undissociated form, the monovalent anionic form, and the divalent anionic form of the dicarboxylic acid, respectively, while H^+ represents a proton.

$K_{a1} = 10^{-pK_{a1}} = [H^+] [HA^-] / [H_2A]$

$K_{a2} = 10^{-pK_{a2}} = [H^+] [A^{2-}] / [HA^-]$

K_{a1} and K_{a2} correspond to the first and second acid dissociation constants of dicarboxylic acids, respectively.

Denominator (D) is as $[H^+]^2 + K_{a1} [H^+] + K_{a1} K_{a2}$

$\alpha_0 = [H^+]^2 / D$

$\alpha_1 = K_{a1} [H^+] / D$

$\alpha_2 = K_{a1} K_{a2} / D$

Furthermore, α_0, α_1, and α_2 represent the fractional abundances of the undissociated species H_2A, the monovalent anion HA^-, and the divalent anion A^{2-}, respectively. The proton concentration is denoted as $[H^+]$, which was taken to be 10^{-7} M at pH 7 and 10^{-4} M at pH 4.

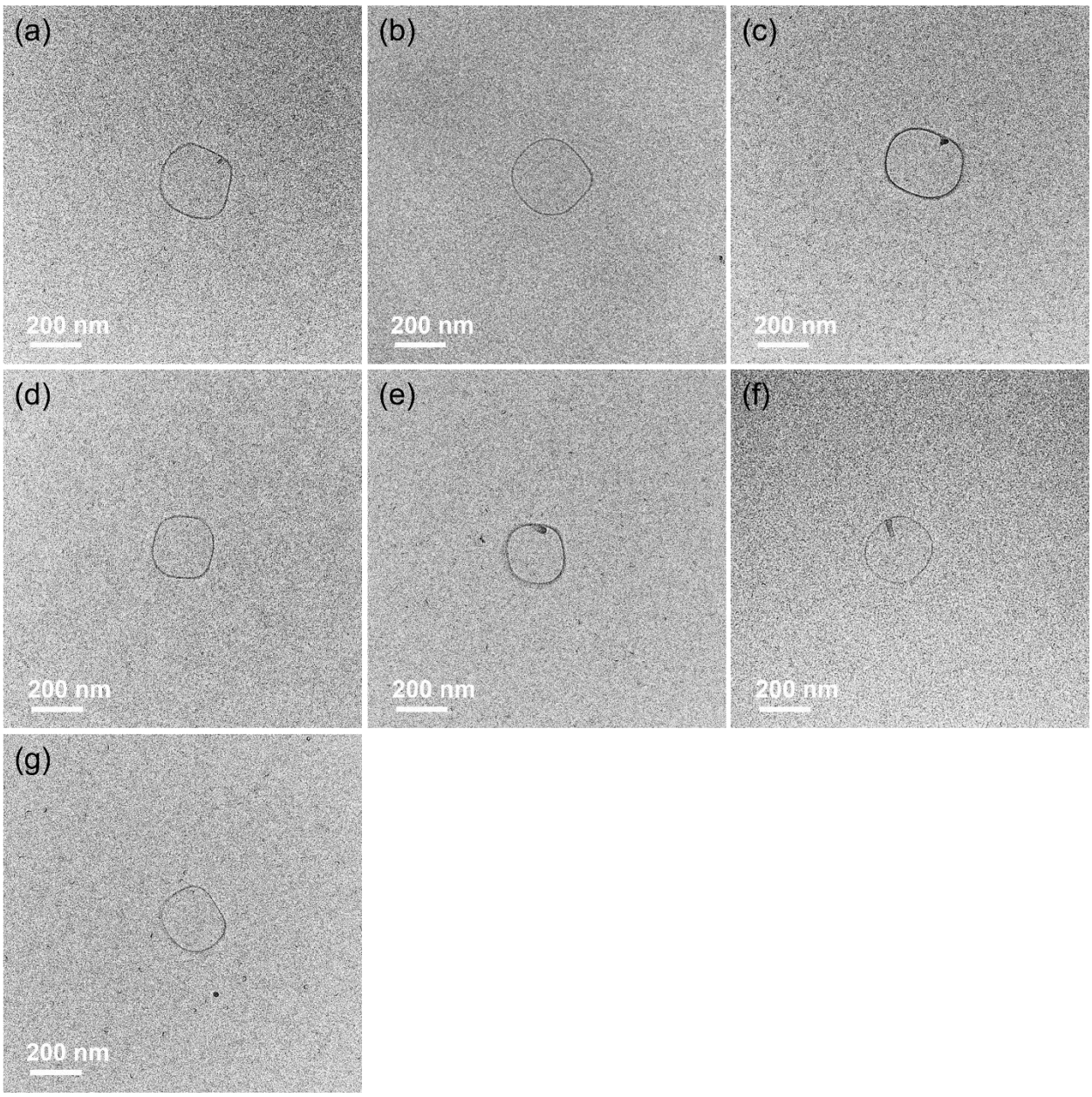

Fig. S4. LC-TEM images of **MEL-A** vesicles (4.7×10^{-4} M) in a pH 7.0 buffer solution containing 3.0×10^{-3} M of (a) oxalic acid, (b) maleic acid, (c) fumaric acid, (d) malonic acid, (e) succinic acid, (f) glutaric acid, and (g) adipic acid.

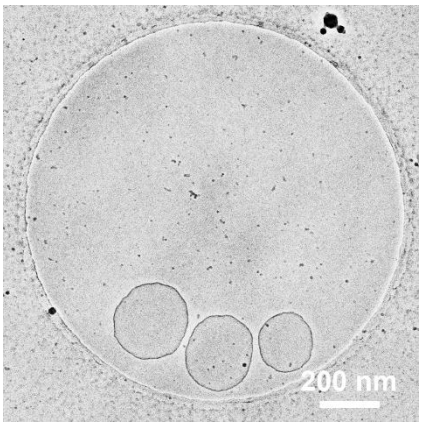

Fig. S5. Representative cryo-TEM image of **MEL-A** vesicles at pH 4 in the presence of propionic acid.

Table S2. Ratio of the third to first vibronic bands (I_3/I_1) of pyrene monomer fluorescence in various solutions at 25°C; [pyrene] = 2.0×10^{-6} M, λ_{ex} = 335 nm

Solution	I_3/I_1 ratio
Water	0.58
Chloroform	0.79
Buffer solution at pH 7 containing 10^{-4} M of **MEL-A**	1.05
Buffer solution at pH 7 containing 10^{-3} M of **MEL-A**	1.05
Buffer solution at pH 4 containing 10^{-4} M of **MEL-A**	1.06
Buffer solution at pH 4 containing 10^{-3} M of **MEL-A**	1.05

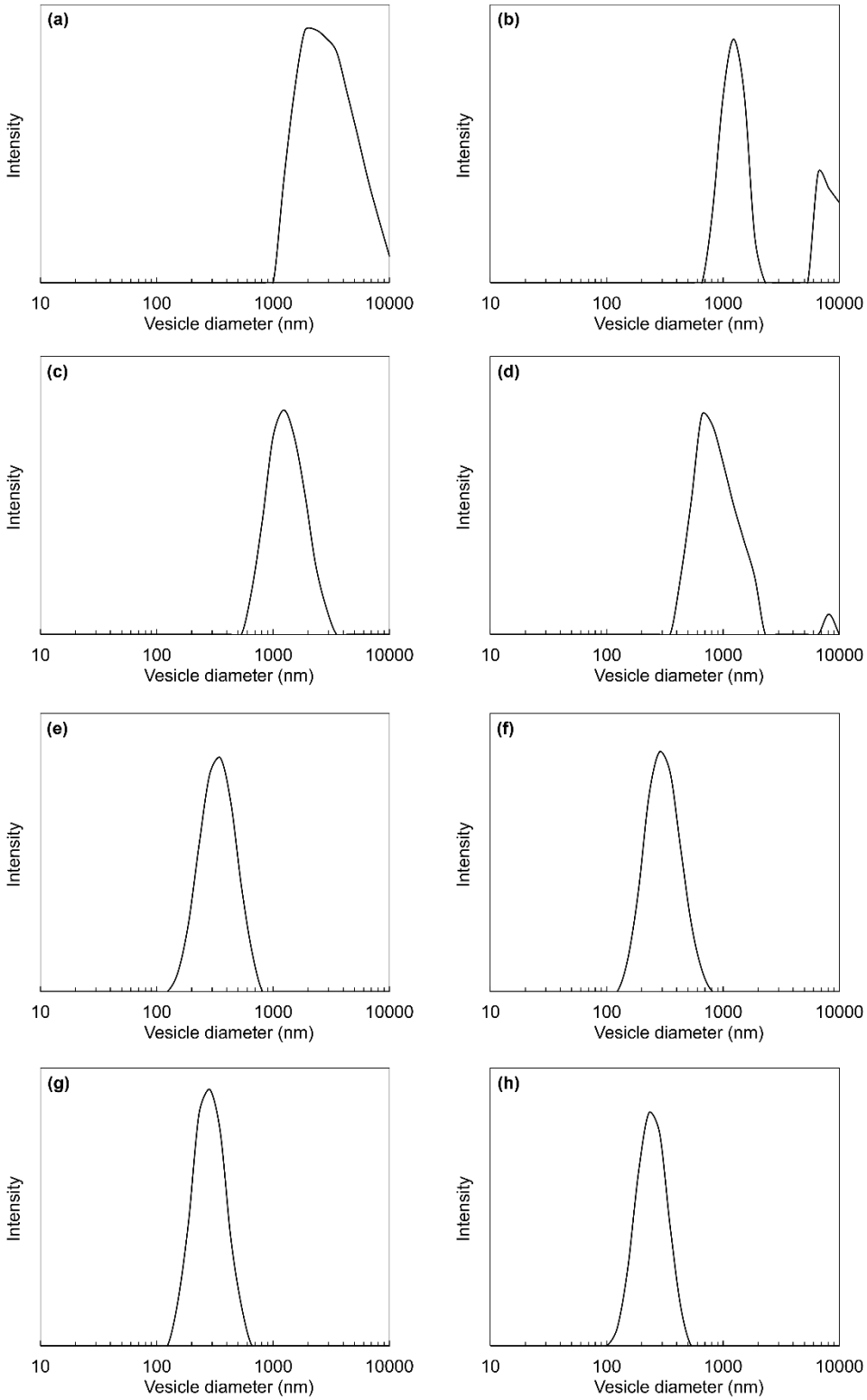

Fig. S6. Vesicle diameter distributions of **MEL-A** assemblies obtained by DLS in the presence of (a) oxalic acid, (b) maleic acid, (c) fumaric acid, (d) malonic acid, (e) succinic acid, (f) glutaric acid, (g) adipic acid, and (h) propionic acid at pH 4. Measurements were carried out at [**MEL-A**] = 4.7×10^{-4} M and [carboxylic acid] = 3.0×10^{-3} M.

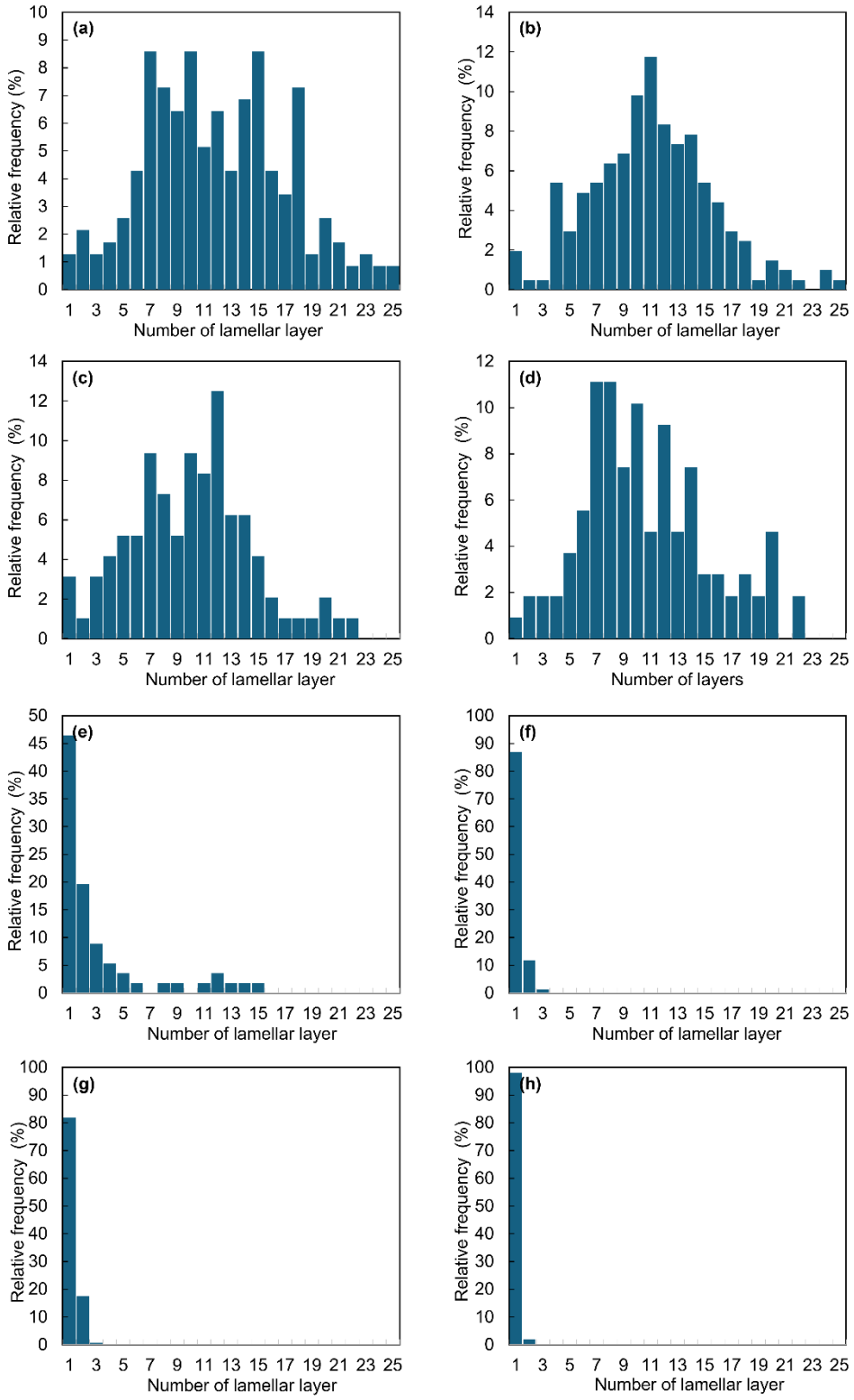

Fig. S7. Lamellar layer number histograms derived from cryo-TEM images of **MEL-A** vesicles in the presence of (a) oxalic acid, (b) maleic acid, (c) fumaric acid, (d) malonic acid, (e) succinic acid, (f) glutaric acid, (g) adipic acid, and (h) propionic acid at pH 4.

References for SI

[S1] T. Morita, M. Konishi, T. Fukuoka, T. Imura, D. Kitamoto, Physiological differences in the formation of the glycolipid biosurfactants, mannosylerythritol lipids, between *Pseudozyma antarctica* and *Pseudozyma aphidis*, *Appl. Microbiol. Biotechnol.*, 2007, **74**, 307–315.

[S2] K. Kalyanasundaram, J. Thomas, Environmental effects on vibronic band intensities in pyrene monomer fluorescence and their application in studies of micellar systems, *J. Am. Chem. Soc.*, 1977, **99**, 2039–2044.

[S3] T. Parasassi, G. D. Stasio, G. Ravagnan, R. M. Rusch and E. Gratton, Quantitation of lipid phases in phospholipid vesicles by the generalized polarization of Laurdan fluorescence, *Biophys. J.*, 1991, **60**, 179–189.

[S4] T. Parasassi, G. Gratton, W. M. Yu, P. Wilson, M. Levi, Two-photon fluorescence microscopy of Laurdan generalized polarization domains in model and natural membranes, *Biophys. J.*, 1997, **72**, 2413–2429.